Combined Visualization of Vessel Deformation and Hemodynamics in Cerebral Aneurysms

Monique Meuschke, Samuel Voss, Oliver Beuing, Bernhard Preim, Kai Lawonn

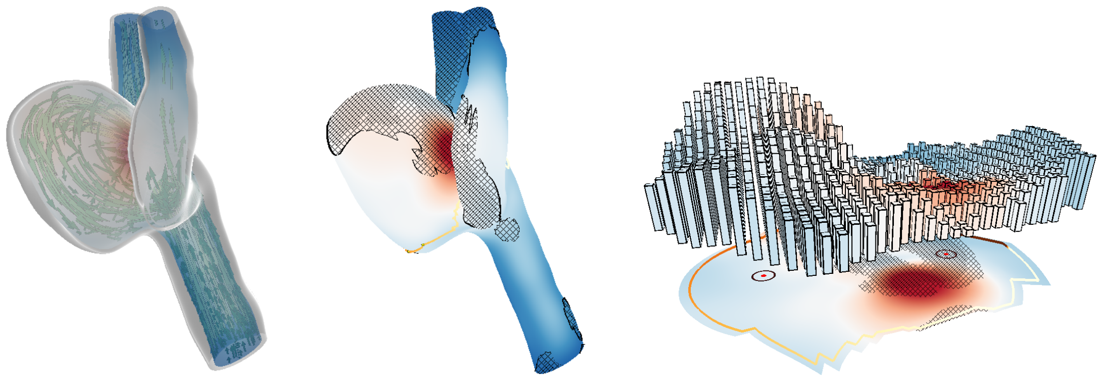

Fig. 1. Depiction of cerebral aneurysm data using a 3D and 2.5D visualization. In 3D the outer and inner vessel wall with internal blood flow is displayed (left). On the inner wall two scalar fields are represented. Here, the wall deformation is color-coded and the Wall Shear Stress is depicted by illustrative techniques (middle). The 2.5D view comprises a 2D map for an occlusion-free visualization of the aneurysm surface and an optional 3D bar chart to depict an additional parameter. In this example, the wall thickness is presented.

Abstract—We present the first visualization tool that combines patient-specific hemodynamics with information about the vessel wall deformation and wall thickness in cerebral aneurysms. Such aneurysms bear the risk of rupture, whereas their treatment also carries considerable risks for the patient. For the patient-specific rupture risk evaluation and treatment analysis, both morphological and hemodynamic data have to be investigated. Medical researchers emphasize the importance of analyzing correlations between wall properties such as the wall deformation and thickness, and hemodynamic attributes like the Wall Shear Stress and near-wall flow. Our method uses a linked 2.5D and 3D depiction of the aneurysm together with blood flow information that enables the simultaneous exploration of wall characteristics and hemodynamic attributes during the cardiac cycle. We thus offer medical researchers an effective visual exploration tool for aneurysm treatment risk assessment. The 2.5D view serves as an overview that comprises a projection of the vessel surface to a 2D map, providing an occlusion-free surface visualization combined with a glyph-based depiction of the local wall thickness. The 3D view represents the focus upon which the data exploration takes place. To support the time-dependent parameter exploration and expert collaboration, a camera path is calculated automatically, where the user can place landmarks for further exploration of the properties. We developed a GPU-based implementation of our visualizations with a flexible interactive data exploration mechanism. We designed our techniques in collaboration with domain experts, and provide details about the evaluation.

Index Terms—Medical visualizations, aneurysms, blood flow, wall thickness, wall deformation, projections

1 Introduction

Cerebral aneurysms are abnormal local dilatations of intracranial arteries, resulting from a pathological weakness in the vessel wall. Their most serious consequence is their rupture, which leads to a subarachnoid hemorrhage and is associated with a high mortality and morbidity rate. In case of a rupture, a therapy is essential. This is different for unintentionally detected aneurysms whose number is rising due to the increased use of Magnetic Resonance Imaging for assessing the patient's state in case of widespread symptoms, e.g., persistent headaches. The detection of a cerebral aneurysm represents a serious dilemma - it has to be communicated to the patient and leads to anxiety. Treatment is often possible, but with a considerable risk of severe complications. Thus, it is highly desirable to better understand the individual risk of an aneurysm and to restrict treatment to high-risk patients. Different factors influence the aneurysm evolution and risk of rupture, such as genetics, vessel morphology, inflammation, and hemodynamic information [6]. Branchings, curved regions, blebs and regions with a low wall thickness [4] are morphological risk indicators. Hemodynamic information are characterized by quantitative parameters such as Wall Shear Stress (WSS), and qualitatively, e.g., with respect to near-wall flow (NWF) and inflow jet. Unfortunately, the processes causing an aneurysm rupture are not well understood. Computational Fluid Dynamic (CFD) simulations and Fluid-Structure Interaction (FSI) enable the investigation of the patient-specific internal wall mechanics and hemodynamics. Therefore, they play an important role in evaluating the rupture risk. Experts are interested in whether there are correlations between hemodynamic parameters that are associated with an increased risk of rupture and high-risk wall regions. The obtained flow data are very complex, which complicates the evaluation of the data.

- *Monique Meuschke is with University of Magdeburg, Germany, and Research Campus STIMULATE. E-mail: meuschke@isg.cs.uni-magdeburg.de.*
- *Samuel Voss is with University of Magdeburg, Germany, and Research Campus STIMULATE. E-mail: samuel.voss@ovgu.de.*
- *Oliver Beuing is with University of Magdeburg, Germany, and Research Campus STIMULATE. E-mail: oliver.beuing@med.ovgu.de.*
- *Bernhard Preim is with University of Magdeburg, Germany, and Research Campus STIMULATE. E-mail: bernhard@isg.cs.uni-magdeburg.de.*
- *Kai Lawonn is with the University of Koblenz-Landau, Germany. E-mail: lawonn@uni-koblenz.de.*

Manuscript received 31 Mar. 2016; accepted 11 Jul. 2016. Date of Publication 23 Oct. 2016; date of current version 12 Jul. 2016. For information on obtaining reprints of this article, please send e-mail to: tvcg@computer.org.

Visualization tools that are capable of presenting all relevant morphology and flow information in an integrated view are thus essential.

Current visualization solutions illustrate either two hemodynamic parameters with the surrounding vessel or depict the wall thickness with one hemodynamic factor, but a combined visualization was not possible so far. Moreover, existing approaches present the aneurysm wall in a rigid manner. However, the vessel deformation is an important factor for the estimation of the rupture risk and should therefore be visualized [32]. We present the first integrated visualization of the vessel morphology considering wall thickness and wall deformation as well as hemodynamic parameters and the internal blood flow based on FSI simulations. It comprises a 2.5D view linked to a 3D depiction of the aneurysm walls such that two parameters can be analyzed simultaneously, see Fig. 1. The 2.5D view combines existing techniques that build up a novel, occlusion-free overview visualization of the aneurysm surface. The 3D visualization represents the focus upon which the exploration of the scalar data and blood flow information over the cardiac cycle takes place. To support the time-dependent parameter analysis, a camera path is calculated automatically. We integrate these techniques into a framework that we developed in collaboration with domain experts. In summary, our main contributions are:

- A linked 2.5D and 3D view of the aneurysm surface for an occlusion-free, simultaneous exploration of morphological and hemodynamic parameters together with the internal blood flow.
- An interactive planning of a camera animation to support the exploration of the time-dependent information.
- A visualization of the wall deformation with wall thickness during the cardiac cycle.
- A report on a qualitative evaluation with domain experts that revealed the advantages of our developed framework.

The rest of the paper is organized as follows. Section 2 provides a survey of related literature. Section 3 and 4 describe the medical background and data acquisition. Section 5 and 6 explain the requirements and implementation of our method. Domain expert evaluation and enhancements to our method are presented in Section 7 and 8. Section 9 concludes the paper with directions of future work.

2 Related Work

Related publications comprise the depiction and exploration of blood flow, especially in aneurysms, and the selection of optimal viewpoints.

Visualization of Blood Flow. Measured and simulated blood flow data are highly complex information whose visualization is often affected by visual clutter and occlusions. Common analysis tools use standard flow visualization techniques such as 3D streamlines, path lines or particle animations. Cross-sectional planes often serve as starting point of the geometry-based methods and show flow information in 2D, e.g., color-coded according to the velocity. However, these techniques need a lot of interaction and rarely address the occlusion problem. Therefore, a variety of tools and visualization techniques were developed that support the visual perception of the patient's hemodynamics. Mattausch et al. [25] presented strategies for the interactive exploration of 3D flow by mapping flow features to different visual attributes such as density and opacity. Van Pelt et al. [42] introduced a framework for the interactive exploration of 4D phase-contrast magnetic resonance imaging (PC-MRI) data that represents cardiac blood flow. They enable an interactive translation of 2D vessel cross-sections that serve as seeding points for the path lines and as planar reformats. Moreover, they used specular highlights on path lines and illustrative renderings like arrow trails to illustrate time-dependent blood flow dynamics. Furthermore, van Pelt et al. [43] developed an approach for interactive virtual probing. The probe can be semi-automatically positioned and the flow behavior is depicted using illustrative techniques like speed lines and particle animations based on elliptical glyphs. These methods cannot assist the user in the interpretation of blood flow concerning specific flow patterns such as vortices or high-velocity jets. Thus, several methods for the extraction and visualization of such features were presented. Salzbrunn et al. [35] introduced *line predicates* that are used to extract interesting flow characteristics including *inflow jets* [5] or vortices [19] in the aorta. Van Pelt et al. [45] applied a hierarchical clustering method to the phase images of aortic 4D PC-MRI data to achieve a more abstract flow depiction. Each cluster is visualized by a representative path arrow. An overview of the visualization of simulated and measured flow data can be found in the summary by Preim and Botha [33].

Visualization and Exploration of Aneurysms. Hastreiter et al. [16] presented a direct volume rendering (DVR) approach of cerebral aneurysms to support diagnosis and intervention planning. For a more objective evaluation of the aneurysm morphology, Tomandl et al. [40] presented a standardized vessel depiction using DVR.

For a combined exploration of the aneurysm morphology and hemodynamic data Neugebauer et al. [29] employed a 2D map projection. With this, a scalar field is used to decode information on the surface and the 2D map. Goubergrits et al. [15] mapped the aneurysm surface to a uniform spherical shape to analyze statistical WSS distributions. While these approaches enable users to explore quantitative parameters, no vectorial blood flow information is provided.

Gasteiger et al. [13] introduced the *FlowLens*, an interactive focus-and-context approach for the simultaneous exploration of anatomical and hemodynamic information. The main drawback of this method is the inability to observe the blood flow outside the area defined by the lens. Therefore, Lawonn et al. [21] provided a vessel visualization technique such that the vessel morphology can be better perceived and the flow information is always visible. Tao et al. [39] presented a web-based interface for the exploration of aneurysm morphology and hemodynamics including a 2D mapping of the aneurysm surface, called *VesselMap*. However, they assumed a rigid aneurysm wall and provide no information about the wall thickness. For a more detailed exploration of flow patterns, Neugebauer et al. [30] developed a qualitative exploration of near-wall hemodynamics in cerebral aneurysms. Several 2D widgets are used to simplify the flow representing streamlines at different positions on the surface. To simplify the flow information, Oeltze et al. [31] compared different state-of-the-art clustering techniques to cluster 3D streamlines representing the blood flow in cerebral aneurysms. Gasteiger et al. [12] applied line predicates to simulated blood flow data of cerebral aneurysms to determine inflow jets and *impingement zones*. Based on this, a comparative visualization for evaluating various stent configurations was presented, integrating the vessel morphology and hemodynamic information [44].

With regard to the wall thickness as an important rupture risk factor, Glaßer et al. [14] presented a framework for the visual exploration of vessels with wall thickness. They visualized the wall thickness combined with hemodynamic information, but a visual representation of the interior blood flow was also missing. Lawonn et al. [22] presented a framework for an occlusion-free blood flow visualization combined with wall thickness information by using illustrative techniques.

Viewpoint Selection. Besides an adequate visualization of scalar parameters, a capable camera control including an adequate viewpoint selection is crucial for an efficient analysis of the complex data. Drucker [10] presented an assortment of camera primitives that enable an intelligent controlling of virtual cameras in computer graphics. Mühler et al. [28] presented a general approach for viewpoint selection in medical surface depictions for intervention planning tasks. Ma et al. [24] focused on the selection of optimal viewpoints for an automatic guide to explore flow features of time-independent vector fields. Vázques et al. [46] introduced the viewpoint entropy as a measure to assess the quality of a viewpoint for general scenes and applied it to imaged-based rendering [47]. Neugebauer et al. [30] used surface parameters such as the curvedness to identify regions of interest (ROIs) for seeding NWF. Related to this, we also derive viewpoints from surface parameters based on thresholds selected by the user.

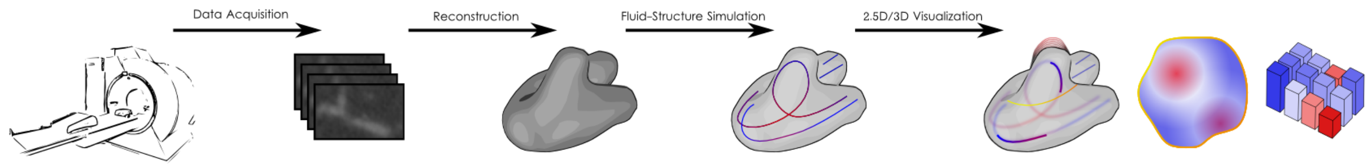

Fig. 2. Overview of our approach to analyze aneurysm data. First, clinical image data is acquired from which the surface mesh is reconstructed as input for the fluid-structure simulation. The rendering and exploration of the simulation results is realized with our 2.5D and 3D view.

3 Medical and Hemodynamic Background

Currently, several morphological features of aneurysms are used to assess their rupture risk, namely their size, shape, location and others [20]. It has been shown that these parameters differ statistically significant between ruptured and unruptured aneurysms. However, the rupture risk of an individual aneurysm cannot be described sufficiently using these criteria, and no information about future changes of the aneurysm morphology or the rupture risk can be derived. Also, it is known that intra-aneurysmal hemodynamics plays a major role in the development, growth and rupture of aneurysms [6]. A promising method to investigate intra-aneurysmal flow is CFD [18]. Several studies found differences of flow patterns in ruptured and unruptured aneurysms, and some flow parameters were directly connected to aneurysm rupture. One quantity that provoked a lot of controversy is the WSS, the frictional force induced by the tangential blood flow at the vessel wall [26]. WSS is described as mechanical trigger for biologic signals regulating the vascular remodeling aiming at homeostasis (stability). Thus, WSS can be rated as an indicator for functional changes in the aneurysm walls, and such changes may either strengthen or weaken the wall. However, rupture occurs when WSS exceeds wall strength. This brings focus to the wall and its properties, which are not considered in classical CFD assuming a rigid wall. Contrary to that, small wall movements due to the pulsatile flow character of the heart were reported [17]. Hence, CFD can be extended by FSI, enabling the analysis of wall deformation and tension. In the past, possible rupture criteria were derived from FSI computations. Sanchez et al. [37] correlate the volume change of aneurysms during the cardiac cycle with the occurrence of rupture. The relation between the material properties and the known rupture site was investigated by Cebral et al. [7]. In essence, FSI is a comprehensive method to determine the interaction of internal wall mechanics and blood flow. The transfer of these new findings from the engineering point of view and biomechanical questions into the clinical discussion is the aim of this paper.

4 Data Acquisition and Preprocessing

In this section, we describe the data acquisition pipeline that consists of four steps, illustrated in Fig. 2.

Acquisition. First, clinical image data including computed tomography angiography, magnetic resonance angiography and 3D rotational angiography of the aneurysm morphology are acquired. Common clinical resolutions are up to $512 \times 512 \times 140$ with a voxel size of $0.35 \times 0.35 \times 0.9$ mm.

Extraction of the 3D Surface Mesh. Based on the image data, the vessel surface is reconstructed using the pipeline by Mönch et al. [27]. Due to the used contrast agents or special sequences, all employed modalities exhibit a high vessel-to-tissue contrast. This facilitates the usage of a threshold-based segmentation followed by a connected component analysis to separate the aneurysm and its parent vessel from the surrounding tissue. The 3D vessel surface is extracted via Marching Cubes, applied to the segmented image data. For the preparation of a geometric model for FSI simulation, it is necessary to manually correct artifacts (details can be found in [27]). Moreover, the mesh quality was optimized by a combination of metric and topological changes such as edge collapses and edge flips [38]. The results are evaluated by medical experts to ensure anatomical plausibility.

Fluid-Structure Simulation. Addressing the FSI simulation, every aneurysm is divided into two subdomains: the fluid and solid domain. CFD is used to calculate the hemodynamics inside the fluid domain numerically. This method makes use of the Navier-Stokes Equations and is widely used for flow characterization in patient-specific aneurysm geometries. Based on the finite-volume method the conservation of mass and momentum is solved locally within each time step. Furthermore, structural simulations are performed to include the vessel wall behavior that is strongly correlated to rupture, assuming that rupture is caused by wall tension that exceeds wall strength. Using the finite-element method, the relation of deformation, mechanical strain and mechanical stress is solved locally for each finite element, based on the conservation of momentum. The deformation of the solid domain reacts on the fluid domain and therefore on the flow characteristics, inducing a complex coupling of both domains. This coupling is located at the interface, the intersecting surface of fluid and solid. This FSI is implemented as data transfer at the interface, exchanging fluid pressure as well as WSS and wall displacement, respectively as updated boundary condition at defined time steps.

Simulation specification. The fluid is modeled as incompressible Newtonian fluid with a density of $1055\,\mathrm{kg/m^3}$ and a dynamic viscosity of $0.004\,\mathrm{Pa\,s}$ [36]. For Case 1 and Case 2, patient-specific velocity profiles are available as inlet boundary conditions [3], lasting 0.93 s and 0.81 s respectively, depending on the heart rate of the patients during acquisition. Due to absence of similar data, these profiles are used for the remaining cases as well. The outlet pressure was defined as zero, since only the relative pressure is calculated. The vessel wall is deformable and couples the fluid domain to the solid domain. The latter is modeled as homogeneous and isotropic using a linear elastic material model, considering a Young's modulus of 1 MPa, the Poisson's ratio is 0.45 and the density is $1050\,\mathrm{kg/m^3}$, as employed in [2, 41]. Simplifications in the choice of the material model coincide with other studies. The wall thickness was assumed to range from 0.2 to 0.6 mm [8, 41] obtained by normal extrusion of the lumen wall, because patient-specific data are not yet widely available. The structure domain is fixed at the inlet and outlets in cross-sectional planes in all directions. All other surfaces are free to move. Table 1 lists the cases and their number of domain-representing cells (fluid) and elements (solid), respectively. The time step for the fluid domain was constantly 0.001 s and for the solid domain maximally 0.01 s. As coupling time step 0.01 s is appropriate to describe the FSI. In every case, two cardiac cycles were simulated, discarding the first and post-processing the second to avoid inaccuracies from initialization. Solvers for the fluid domain were STAR-CCM+ (CD-adapco, USA) and for the structure domain Abaqus FEA (Dassault Systèmes Simulia Corp., USA). All calculations were performed on a standard workstation (using four Intel Xeon E3 cores with 3.3 GHz and 32 GB RAM) and lasted between 4 and 16 hours, depending on its complexity.

Table 1. Spatial resolution and CPU time of FSI computations.

Case	Cells (fluid)	Elements (solid)	CPU time in s
1	291 738	55 068	27 820
2	252 429	63 132	21 841
3	236 882	64 816	16 178
4	368 958	137 980	36 652
5	342 925	113 475	55 912

Post-processing. This includes the mapping of cell-based variables to the vertices and path line integration for the fluid domain. Every 0.01 s 100 path lines are emitted at the cross-sectional area where the fluid enters the solid domain using a Runge-Kutta-4 integration.

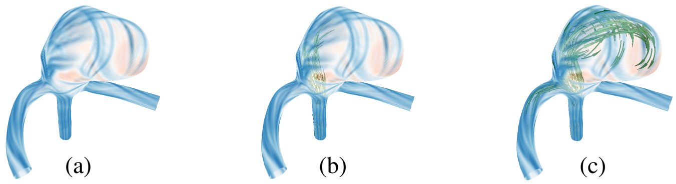

Fig. 3. Visualization of the NWF for Case 1. The inner vessel wall is depicted semi-transparently with a color-coding of the NWF (a). Blue areas indicate that flow comes close to the wall, whereas in red regions the path lines have a greater distance to the wall. Due to the global distance measurement over the cardiac cycle, the path lines follow the blue stripes on the wall that display NWF regions (b-c).

5 Requirement Analysis

For developing a visualization framework that is able to depict the wall deformation and wall thickness together with hemodynamic parameters and animated blood flow several requirements need to be fulfilled. Our approach is based on discussions with two domain experts: one neuroradiologist with 16 years of work experience and one CFD engineer working on FSI simulations for cerebral aneurysms with three years of work experience. Additionally, the neuroradiologist treats cerebral aneurysms regularly and is involved in clinical research on the investigation of the risk of rupture.

The aim of the experts is to better understand the risk of rupture. Particularly interesting is the simulation of ruptured aneurysms before and after rupture. The experts are trying to find parameter characteristics and correlations that might have caused the rupture. Such analysis should lead to a patient-specific assessment of rupture risk in the future. To define requirements, we discussed the previous procedure to explore the aneurysm data and occurring difficulties with the experts. For the parameter exploration, the scalar data is color-coded on the 3D aneurysm surface. Depending on the chosen parameter, they search manually for conspicuous parameter values, especially at irregular shapes of the vessel wall, e. g., blebs, which are additional bulges on the aneurysm. Such vessel wall changes indicate remodeling due to plaques, which are inflammatory changes in blood vessels and are essential to assess the risk of rupture. Moreover, both experts explain that strong local changes of the vessel deformation and wall thickness are important. Since the surface morphology and the flow behavior influence each other, the experts stated that an integrated view of both characteristics is needed. To explore the hemodynamics, the aneurysm surface is depicted semi-transparently and the internal blood flow is represented by animated path lines. Moreover, the experts want to know the distance of the flow near the wall, because it may lead to further pathological vessel dilation. Therefore, they try to visually approximate the distance of the path lines to the vessel wall.

However, the experts consider the sole presentation of a 3D model as not sufficient, since important information can be occluded. Due to the complexity of the surface, a series of manual rotations is necessary to gain a complete overview. The time-dependent behavior of the data further enhances the manual exploration effort, because it is almost impossible to find critical regions during animation, since the rotation process itself needs a certain amount of time. Moreover, only one parameter can be displayed simultaneously. During rotation and zooming, the experts switch scalar quantities such that different interesting regions are found. Thus, the experts have to memorize the regions and analyze them regarding other quantities as well, which makes the detection of critical parameter correlations very time-consuming. For more complex vascular branches, the number of ROIs and occlusion problems increases such that a full analysis of various scalar values becomes quite challenging. In addition, they describe the approximation of the distance between vessel wall and flow as very demanding and error-prone, because again considerable rotation effort is needed. They wished a visualization that enables a fast and simple evaluation of morphological and mechanical wall properties as well as hemodynamic parameters and their correlations. Besides the 3D surface representation, they need an occlusion-free depiction, which gives a fast overview about the complex data. Based on these discussions and our analysis of the state of the art, we summarize the main requirements for the visual exploration of vessel characteristics as follows:

Req. 1 Vessel view with wall deformation and thickness. We need an occlusion-free visualization, comprising the vessel morphology as well as information about the wall deformation and thickness, which serves as overview depiction. To facilitate a semi-quantification for the detection of dangerous regions, e.g., at thin vessel regions, a discrete color scale should be provided.

Req. 2 Depiction of NWF. The blood flow needs to be visible during the whole animation. Moreover, the experts are interested in the distance of the flow to the vessel wall.

Req. 3 Simultaneous exploration of parameters. The experts want to evaluate whether local changes of hemodynamic parameters occur on morphologically abnormal wall sections or not. Therefore, a visualization is needed that enables the simultaneous analysis of at least two parameters to identify correlations between them.

Req. 4 Animations for data exploration. Due to the complexity of time-dependent aneurysm data, their exploration should be supported by animations. To simplify the data analysis, an automatic camera movement passing interesting vessel regions should be provided.

Req. 5 Collaboration tools. For collaboration purposes it should be possible to set landmarks in different animation steps. An external researcher should be able to analyze the regions around the landmarks and discuss them with other colleagues.

6 Focus-Context Visualization of Vessel Morphology and Hemodynamic Data

In this section, we describe the implementation of our visualization framework. First, we introduce the 2.5D and 3D aneurysm visualization. Then, we describe the realization of the camera animation and finally we address the collaborative tools.

6.1 Scalar Fields

In consultations with our domain experts, we distinguish eight parameters that can be explored on the aneurysm surface to detect rupture-prone regions and to uncover high-risk parameter correlations. These parameters comprise hemodynamic and morphological information, which can potentially be extended if necessary.

Hemodynamics. With regard to the patient-specific hemodynamics, we enable the exploration of the pressure, which is one of the most important quantities to describe the flow field. Furthermore, the tension inside the wall is depicted to visualize the load which is induced by the hemodynamics. For this, the local stress tensor is converted to a scalar value using the common stress theory of von Mises (like in [41]). Moreover, the WSS as well as the NWF can be explored (Req. 2). Therefore, we determine for each vertex of the surface mesh the nearest path line point using the Euclidean distance. Finally, we took for each vertex the minimum over all path line points independent of the time steps to represent the global near-wall flow. This enables a visualization that depicts the trace of the path lines over time. Fig. 3 shows the NWF using a color-coding. Blue regions indicate flow that comes close to the wall, whereas in red regions the flow has a greater distance to the wall, based on the path lines. Regions where the flow is more distant to the wall indicate that there are thickenings of the inner wall due to the formation of a thrombus or inflammation processes stated by our neuroradiological expert.

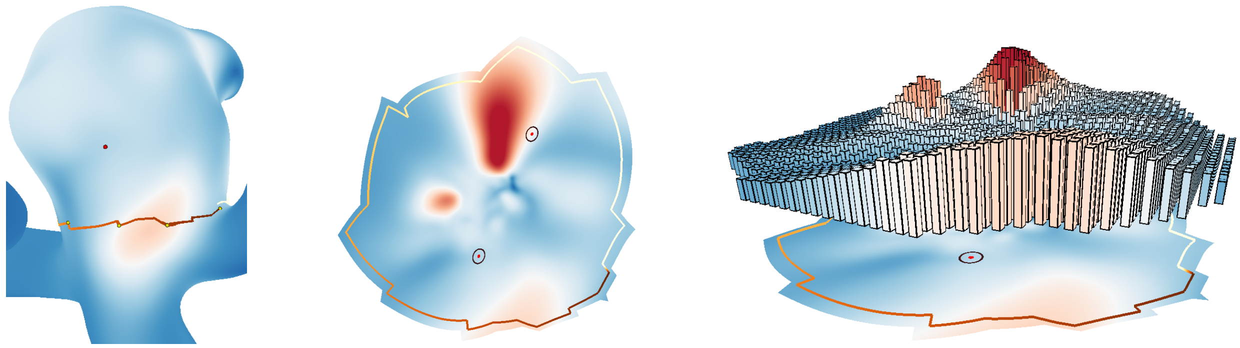

(a) (b) (c)

Fig. 4. 2.5D depiction of Case 4. For the 2D map generation, the user defines markers along the aneurysm ostium that are connected to a cut line and two markers on the dome (one is depicted as red point). The surface is unfolded where the dome markers and the ostium were emphasized in the map (b). Moreover, the map is sampled to calculate bar charts (c). Here, the deformation is mapped to color and height of the bars.

Morphology. The morphological parameters comprise the wall thickness and wall deformation. Moreover, we identify interesting regions such as blebs based on the curvature measures, similar to Neugebauer et al. [30]. For this, we employed the *shape index* as well as the *curvedness scalar*. The curvature is calculated with the algorithm of Rusinkiwicz [34]. For every triangle, he estimates the shape operator by defining the deviation of the normal along every edge. This provides an equation system which can be numerically approximated by the method of least squares. Afterwards, the shape operator is accumulated for every vertex by taking the operator of the incident triangles into account. The eigenvalues of the shape operator yield the principle curvature values κ_1, κ_2 of every point. Given the curvature measures, the shape index is computed as

$$s = \frac{1}{2} - \frac{1}{\pi} \tan -1 \frac{\kappa_1 + \kappa_2}{\kappa_1 - \kappa_2}, \tag{1}$$

with $\kappa_1 \geq \kappa_2$. The shape index ranges from 0 to 1, where 0 stands for a cup-shaped and 1 for a cap-shaped form. The curvedness is given by

$$c = \sqrt{\frac{\kappa_1^2 + \kappa_2^2}{2}}. \tag{2}$$

6.2 2.5D Aneurysm Overview

Scalar quantities, such as pressure, WSS or wall thickness, play a major role in the risk assessment of cerebral aneurysms. Their previous exploration on the 3D aneurysm surface is very time-consuming and mentally exhausting due to the complexity of the data (recall Section 5). The simultaneous parameter analysis could be supported by using side-by-side views. However, this would only allow the analysis of a small amount of time steps or parameters, but it is still difficult to mentally combine these multiple images. Thus, providing visualization techniques to clearly display these scalar values and their correlations is quite important.

As a remedy, we provide a novel 2.5D visualization as a combination of existing visualization methods that ensures a fast overview such that the distribution of a chosen scalar quantity can be explored without any occlusions (Req. 1). Similar to Neugebauer et al. [29], we use a map to display the information, which is inspired by other medical overview techniques, such as colon and brain flattening as well as the more abstract bull's eye plot used in cardiology. In contrary, we did not visualize the map in combination with the 3D render context, but in an additional render context to avoid visual clutter. The map is determined with a parametrization algorithm that maps every point $\mathbf{p}_i \in \mathbb{R}^3$ on the surface mesh to a point $\mathbf{u}_i \in \mathbb{R}^2$ in the plane. We employed the algorithm *least squares conformal maps* to obtain a 2D overview visualization [23]. We used this approach as it is boundary-free. We only need to set two points as constraints for the parametrization.

In the following, we shortly recap the algorithm. Let (i, j, k) be the vertex indices of a triangle in the surface mesh and let $\mathbf{p}_i \in \mathbb{R}^3$ denote the corresponding position of the vertex with index i. For every triangle, an orthonormal basis $\mathbf{e}_1, \mathbf{e}_2$ is determined by

$$\mathbf{e}_1 = \frac{\mathbf{p}_j - \mathbf{p}_i}{\|\mathbf{p}_j - \mathbf{p}_i\|}, \mathbf{n} = \frac{\mathbf{e}_1 \times (\mathbf{p}_k - \mathbf{p}_i)}{|\mathbf{e}_1 \times (\mathbf{p}_k - \mathbf{p}_i)|}, \mathbf{e}_2 = \mathbf{n} \times \mathbf{e}_1. \tag{3}$$

Then, the gradient with the basis $\mathbf{e}_1, \mathbf{e}_2$ is given by

$$\nabla u = \underbrace{\frac{1}{2A_T} \begin{pmatrix} \mathbf{e}_2^j - \mathbf{e}_2^k & \mathbf{e}_2^k - \mathbf{e}_2^i & \mathbf{e}_2^i - \mathbf{e}_2^j \\ \mathbf{e}_1^k - \mathbf{e}_1^j & \mathbf{e}_1^i - \mathbf{e}_1^k & \mathbf{e}_1^j - \mathbf{e}_1^i \end{pmatrix}}_{G_T} \begin{pmatrix} u_i \\ u_j \\ u_k \end{pmatrix}, \tag{4}$$

where A_T denotes the area of the triangle and u_i, u_j, and u_k denotes the u coordinate of the vertex point i, j, and k, respectively. Mainly, the *least squares conformal maps* are based on the conformality condition that states that the gradients of the coordinates are orthogonal

$$\nabla v = (\nabla u)^{\perp}, \tag{5}$$

where $\perp$ denotes the counterclockwise rotation of 90 degrees around the normal $\mathbf{n}$. The *least squares conformal maps* minimize an energy E that punishes triangles that do not fulfill the conformality condition:

$$E = \sum_{T=(I,j,k)} A_T \| G_T \begin{pmatrix} v_i \\ v_j \\ v_k \end{pmatrix} - \left(G_T \begin{pmatrix} u_i \\ u_j \\ u_k \end{pmatrix} \right)^{\perp} \|. \tag{6}$$

It is necessary to fix the coordinates of at least two points to have a well-defined optimization problem. In our framework, we implemented an interaction scheme to add the constraint points. First, we ask the user to place markers on the mesh, e.g., the ostium, see Fig. 4(a). These markers will be connected by the Dijkstra algorithm in consecutive order. Afterwards, we cut the mesh along this curve, where the cut line is color-coded on the 3D mesh and the map to establish a spatial correlation between both views, see Fig. 4(b). Then, the user has to place two landmarks as constraints that are mapped to (0,0) and (0,1). For our datasets, we included a preset of points to generate the parametrization. To choose different points is up to the user.

Bar Charts. Based on the discussions with our experts, it is helpful to explore the wall thickness or deformation in combination with two other scalar fields to better understand the role of wall morphology in the rupture risk assessment. To display a third scalar field, we included a 3D bar chart besides visualizing scalar quantities to the 2D map. By default, the height of the bar charts represents the wall thickness, see Fig. 4(c). However, other parameters can be set as well. To

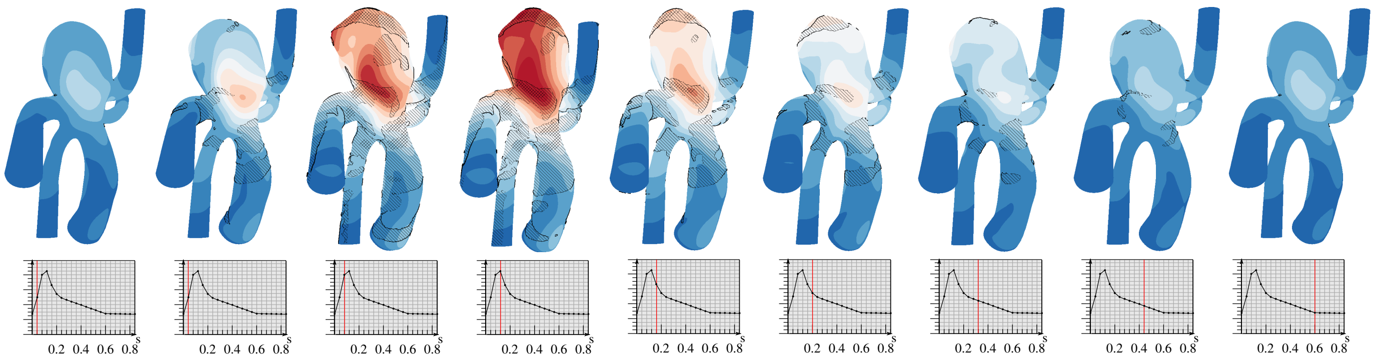

Fig. 5. The wall deformation is color-coded on the aneurysm surface (Case 5) during the cardiac cycle. Furthermore, the WSS is depicted by isolines and hatching, where a threshold of 22,3 Pa was selected. Until the peak of the systole (until 0.2 s) the deformation and WSS increase continuously, while during the systolic end and diastole both parameters decrease.

obtain a regular distribution of the bar charts, we sampled the 2D map regularly. Afterwards, we take only grid points into account which lie inside the 2D map. We ensure this by checking if the grid points lie inside a triangle. Afterwards, we calculate the barycentric coordinates of the grid points with the corresponding triangle. We use the barycentric coordinates to interpolate the chosen scalar field to the grid point. To generate the bars, we employ triangle strips on the GPU and construct a cuboid. Adding an outline for the edges emphasizes the bars and avoids visual clutter. The bar charts indicate immediately whether there are local maxima or minima of the chosen scalar parameter, which could be possible rupture areas, e.g., thin wall regions. The user can then further explore these regions in the 3D view.

6.3 3D Aneurysm Visualization

The 3D aneurysm view enables a detailed parameter exploration. Besides a depiction of the wall thickness, different scalar parameters and inner blood flow, we incorporate the dynamic vessel motion during the cardiac cycle (meet Req. 1). Based on FSI simulations, for each vertex of the surface mesh a deformation vector is known. This information at each time step is used to displace the vertices during the animation.

Vessel Visualization. The visualization of the vessel wall is divided into the depiction of the outer and the inner vessel wall. For the display of the outer vessel wall, we apply the technique presented by Glaßer et al. [14]. For this, the transparency depends on the shading term $\alpha = 1 - \langle \mathbf{n}, \mathbf{v} \rangle$, where $\mathbf{n}$ denotes the normal and $\mathbf{v}$ the view direction of the camera, see Fig. 1. In case the camera faces towards the surface, e.g., $\mathbf{n}$ and $\mathbf{v}$ align, the surface is transparent. If $\mathbf{v}$ is perpendicular to $\mathbf{n}$, the mesh appears more opaque. This technique enhances the spatial impression of the surface (see the evaluation by Baer et al. [1]). On the inner vessel wall the exploration of the scalar data takes place. To enable a depiction of the internal blood flow, the inner wall is visualized semi-transparently. However, the user can adjust the transparency to his/her needs. In the following section, we describe the depiction of the scalar data.

Scalar field visualization. According to Req. 3, a visualization is needed that enables the simultaneous exploration of two parameters. We decided to map the first parameter to a discretized cool-to-warm color scale. Lower values are mapped to a bluish color and higher values to a reddish color. Five colors are used to represent the chosen parameter. However, the user can adapt the number of discretized colors to his/her own needs or select a linear color-coding. The second parameter is visualized by an isoline representation. For this, the user selects the second scalar field and a parameter needs to be set. This parameter serves as a threshold, such that depending on the type of the scalar field, either lower or higher values are emphasized. For example, if the domain experts select the wall thickness, they are interested in values that fall below the threshold, whereas in case of WSS they are interested in regions that are greater than the threshold. The depiction of the region is done by an image-based hatching scheme introduced by Lawonn et al. [22]. In contrast, higher (lower) values are emphasized with a greater number of lines and cross-hatches.

Thus, the experts can set two scalar fields, e.g., wall deformation and WSS, to display ROIs with a high deformation and high WSS values, see Fig. 5. Here, the deformation is color-coded for different time steps, where the diagram below shows the deformation changing during the cardiac cycle and the red bar indicates the current time step. Moreover, the WSS is depicted by an isoline and hatching. Until the systolic peak (until 0.2 s) the deformation increases, indicated by the red regions, and also an increased WSS exists. Afterwards, both parameters decrease and are constantly low during diastole (0.27-0.81 s). Fig. 7(a) shows another example of data exploration. Here, the wall thickness is color-coded and the WSS is represented by an isoline. The user depicted a ROI with low wall thickness and high WSS values. The blue region indicates a thin wall, where high WSS values exist, which is a high-risk rupture area. Moreover, the scalar data is also visualized in the 2.5D depiction using color-coding and illustrative techniques, see Fig. 1 (right).

Path Line Visualization. The path lines are visualized by using an arrow glyph and by color. Inspired by Everts et al. [11], we constructed a view-aligned quad on the GPU to depict the path lines. The successive path line points p_i and p_{i+1} are used to determine the normalized tangent vector: $\mathbf{t} = \mathbf{p}_{i+1} - \mathbf{p}_i$. With the given view direction $\mathbf{v}$ (of the camera), we calculate the extent of the path lines by using the normalized cross-product $\mathbf{e} = \mathbf{v} \times \mathbf{t}$. Then, we parametrize the path lines with two parameters. The first parameter is the current animation time of the cardiac cycle and, thus, similar to the approach by Lawonn et al. [22]. The second parameter is set for the extent and is in the range of $[-1, 1]$. Using the parametrization allows to draw arrow glyphs on the path lines. An offset for the current time is set and gives the range of the current path line part. The start and end points are used to construct the arrow, see [11, 22]. This approach allows an easy interpretation of the speed. If the animation pauses, the length of the depicted path line part corresponds to the speed. Furthermore, another value, e.g., the pressure can be visualized by a color scheme. For this, we used a dark green to light yellow colormap, see Fig. 3.

6.4 Linking between 2.5D and 3D View

To facilitate the correlation between the 2.5D and 3D view, we provide a linking between them. With regard to the direction from 2D to 3D, the user can pick a specific point in the 2D map and the camera rotates automatically to the corresponding 3D position in a smooth way. In 3D, this point is presented as a green sphere at the corresponding position. Thus, interesting regions were presented to the user without a manual search. Furthermore, we integrate a brushing for the 2D map. Instead of picking specific points, the user can brush in the map and the corresponding 3D regions are emphasized by hatching. The brush radius can be controlled with the mouse wheel. Moreover, we integrate a highlighting of 3D regions in the 2D map depending on the zoom level. The closer the user zooms into the 3D scene, the more opaque

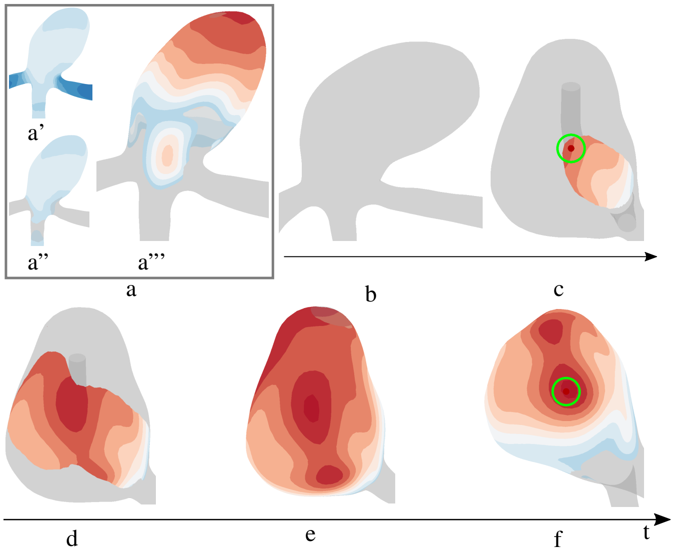

Fig. 6. Generation of an automatic camera animation for Case 1 to identify regions with high pressure and deformation. To restrict the camera path to that regions, two thresholds have to be selected. Based on the color-coded pressure field (a'), the user selects a threshold (a"). Then, the deformation field is color-coded for the second threshold selection (a"'), before the camera animation starts. In the first time step, no candidate was found (b). But in the following two time steps, two candidates were approached, indicated by a green circle (c, f). During the animation (d, e), all surface areas were color-coded that satisfy the thresholds.

the corresponding 2D region is depicted. This supports the perceived spatial correspondence between a 3D region and its related 2D area.

6.5 Camera Animation

To support the user with the exploration and analysis of the data set, we implemented an automatic camera animation that presents the most interesting regions based on the input data of the user (Req. 4). Our experts preferred smooth camera animations over key frames, because they found them easier to comprehend. For this, the user is asked to set various thresholds for different scalar fields. Here, the user selects scalar fields $s_1, s_2, \dots, s_n$ that he/she is interested in. Then, for every scalar field a threshold t_i is set. The selection of the scalar fields with the thresholds leads to a constrained region on the mesh that fulfills every criterion:

$$P = \bigcap_{i=1}^{n} \{p \,|\, s_i(p) \geq t_i\} \tag{7}$$

Note that we wrote $s_i(p) \geq t_i$, but for the scalar fields wall thickness and NWF should be used less equal. The obtained points restrict the camera path. The thresholds can be set independently from each other, where the surface regions that fulfill all selected thresholds were presented using the cool-to-warm color scheme. Regions that do not comply with the thresholds are depicted in gray. Fig. 6 (a) shows an example of the threshold selection. The user starts by choosing the pressure scalar field during systole, which is color-coded on the surface (a') and regions are interactively grayed according to the threshold (a"). Based on the first selection result, the user adjusts a threshold for the deformation, which is now color-coded on the surface (a"'). Finally, regions that satisfy both conditions are used to plan the camera path.

To determine positions for the camera animation, we select candidates that are highly interesting for the user to explore. Thus, the user selects a focus scalar field s_{focus}. Then, candidates are determined, which are first based on the points P (recall Eq. 7) and on s_{focus}. The ordered points P_o, i.e., $s_{focus}(P_o^i) \geq s_{focus}(P_o^{i+1})$ serve as candidates for the camera path. For every time step, we use P_o^0 as the ideal candidate. Thus, we need the position of the camera such that it shows the candidate. For this, we use the position of the candidate and add the normal scaled with a user-defined value. We used $1/10$ of the diagonal of the bounding box as the scalar. With smaller values, the camera came too close to the surface and with greater values the camera was too far away. The view direction of the camera is set such that it points in direction of the candidate. From one point in time to the next, we move the camera to the candidate such that the animation stops before the next point in time is reached. This enables a smooth animation path between the best candidates at different points in time. In case the domain expert is especially interested in various candidates at a specific point in time, e.g., the systole, he/she can start the local camera path. If the local camera path is activated, the animation time is paused and the camera moves beginning from the first candidate to the next ordered points. The candidate is in general highlighted with a circle around a point that indicates its position. Fig. 6 shows an example of the camera animation for three adjacent time steps. In the first time step, no point fulfills the selected thresholds, which results in the gray aneurysm depiction, see Fig. 6(b). In the next time step, the camera rotates automatically to the most interesting point, which is highlighted by a green circle, see Fig. 6(c). Afterwards, the camera rotates to the next candidate (Fig. 6(f)), while all surface regions were color-coded that also fulfill the thresholds (Fig. 6(d, e)).

Mostly, the domain experts are interested in regions on the aneurysm. Therefore, we offer the possibility to restrict the region by an approach that determines the geodesic distance on the surface. For this, the user is asked to place a start point on the aneurysm. Following the method by Crane et al. [9], we compute the distance by solving standard linear elliptic equations. First, the heat flow is integrated $\dot{u} = \Delta u$ for a fixed time t. The second step is to compute the normalized gradient of the evaluated heat flow u: $X = -\nabla u / |\nabla u|$. Finally, the Poisson equation is solved $\Delta \varphi = \nabla \cdot X$, which yields the geodesic distance from the start point on the surface. Afterwards, the user can specify the distance that restricts the region for the camera path. Moreover, brushed regions in the 2D map can also be used to define regions for the camera path.

6.6 Collaboration Tools

To support the collaboration between domain experts, we allow the user to place landmarks on the vessel surface (Req. 5). Each landmark gets an individual color and an individual label can be set, see Fig. 7 (b). Therefore, a textual description of each landmark is available, e.g., for documentation. After the placement, a screenshot is taken and all selected parameters as well as the camera settings are stored. Another expert can see the landmarks on the surface and they are listed together with their labels as a preview in the top right corner. Selecting a landmark in the preview loads the corresponding scene. Landmarks can also be placed if the automatic camera animation is active. During placing and labeling a mark, the camera animation stops and continues after pressing the enter button.

7 Evaluation

For the evaluation of our combined aneurysm visualization, we conducted a user study with five unpaid participants (1 female, 4 male; 28-48 years old; median 35 years). Among them were the two domain experts (both co-authors of this paper) that helped us to define the visualization concept: two physicians (14 and 15 years of experience in radiology) and two CFD engineers involved in hemodynamic analysis (three and six years of professional experience). Furthermore, we added one expert for medical visualization (four years of work experience). At the beginning of the study, we briefly demonstrated our tool and described the functionality to the experts. Afterwards, each feature was explained in more detail and the participants were encouraged to explore the framework on their own. During exploration, we noted the experts' spoken comments and their interaction with the tool. They had to try both views and the bidirectional connection between them as well as the camera animation to find suspicious regions. Finally, we asked them to answer a questionnaire.

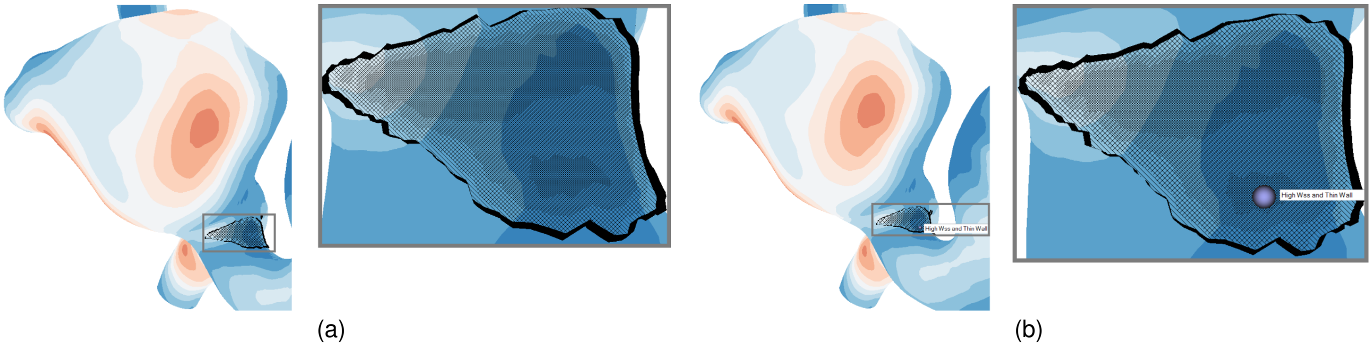

Fig. 7. A domain expert detected a suspicious surface region for Case 2, where the wall thickness is very thin and a high WSS exists (a). He created a landmark at this region and assigned an individual label, represented as purple sphere (b).

7.1 Questionnaire

The questionnaire comprises mainly aspects about our visualization concept and its medical relevance as well as the camera animation. Besides open-ended comments, we asked questions that had to be answered using a five-point Likert scale ($--$, $-$, $\circ$, $+$, $++$). First, we asked for the experts' background and their opinion about the medical relevance of visualizing wall thickness and deformation in combination with blood flow information. Afterwards, they were asked to assess the suitability of the 3D and 2.5D depiction to explore the aneurysm data. Therefore, they should also evaluate techniques to visualize the wall thickness. Finally, the experts commented on the suitability of the camera animation and landmark placement to support the data exploration and collaboration between experts. For further details, we provide the questionnaire as supplemental material.

7.2 Results

In this section, we present the results of our user study, which was performed on a standard desktop computer with an Intel Core i5 with 2.8 GHz, 16 GB RAM, and an NVidia GeForce GTX 560 Ti. For all presented models we achieve a real-time performance of approximately 40 fps, except for the initial calculation of the 2D map with a computation time per case between 9 and 14 s, depending on the amount of triangles. This performance test was conducted with a resolution of 1920 × 1080 and both views (3D and 2.5D view) covered approximately half of this resolution. For the interpretation of our predefined Likert score categories, we provide the number S of experts who chose the individual categories. The overall result of the empirical evaluation is shown in Fig. 8.

Medical Relevance. All domain experts confirmed the high importance of analyzing the wall thickness ($S(++) = 4$; $S(+) = 1$) and wall deformation ($S(++) = 4$; $S(+) = 1$) for the rupture risk assessment in cerebral aneurysms. They also stated that the combined evaluation of wall thickness and deformation together with different hemodynamic parameters is important to identify rupture risk-related correlations ($S(++) = 3$; $S(+) = 2$). Moreover, they emphasized the importance of the data exploration during the whole cardiac cycle instead of just the systolic part, because it is unknown if the aneurysm rupture risk is higher at the systole or diastole.

3D Visualization. All participants confirmed that the combination of color-coding and illustrative techniques enables the simultaneous exploration of two scalar parameters on the aneurysm surface ($S(++) = 3$; $S(+) = 2$). Two participants wished to have an additional path line filtering, e.g., vortex-representing path lines or path lines with high velocity. This would enable an exploration of specific flow patterns, which are reported to be indicators of a high rupture risk. The usefulness of the color-coding on the surface to highlight the NWF was rated by the experts with $S(++) = 3$ and $S(+) = 2$. Moreover, they stated that the surface transparency reveals the qualitative flow behavior ($S(++) = 4$ and $S(+) = 1$).

2.5D Visualization. All participants found that the 2.5D depiction provides a fast overview about the data ($S(++) = 3$; $S(+) = 2$). Moreover, all experts commented that the shape of the map together with the color-coding of the ostium enable to establish a visual correspondence between both views ($S(++) = 4$; $S(+) = 1$). Furthermore, the selection of individual points on the map, followed by changing the camera in 3D, was described as helpful ($S(++) = 2$; $S(+) = 3$).

Wall Thickness Visualization. The semi-transparent representation of the outer wall was rated as least suitable by most participants for the assessment of the wall thickness ($S(+) = 2$; $S(\circ) = 2$; $S(-) = 1$). The perceived thickness depends strongly on the perspective to the surface and requires a lot of manual rotation effort. In contrast, both the color-coding as well as the illustrative rendering were valued with $S(++) = 3$ and $S(+) = 2$. The bar charts were also perceived as very appropriate to assess the local wall thickness ($S(++) = 2$; $S(+) = 3$). Two participants indicated that the bar charts immediately communicate whether there are local minima or maxima, but the indication of the corresponding 3D position should be improved, e.g., by using brushing on the bar charts.

Animation Aspects. Regarding the camera animation, we provide three ways to define candidates on the aneurysm surface. The participants preferred the threshold-based selection ($S(++) = 2$; $S(+) = 3$). The ROI selection and the brushing were rated in the same way with $S(++) = 2$, $S(+) = 2$ and $S(\circ) = 1$. One participant noted that the illustrative rendering of the brushing area in 3D leads to a decreasing spatial impression of the surface. Instead, he suggested a simple outline of the corresponding 3D region. The experts describe the animated camera path as helpful for the exploration ($S(++) = 3$; $S(+) = 2$) of the time-dependent data. Moreover, three participants described the camera path as helpful for the navigation in 3D, whereas the other experts preferred a manual camera rotation together with the animation play bar for navigation ($S(++) = 1$; $S(+) = 2$ and $S(\circ) = 2$). Here, it depends on which part of the aneurysm the users want to navigate their way around. If the users only want to navigate in a small region such as a bleb, a manual rotation was preferred. But for the time-dependent navigation over the whole aneurysm surface, the experts preferred the automatic rotation. One participant wished to have a key interaction for the temporal forward and backward exploration of the candidate points instead of a time bar.

Collaboration Aspects. All experts appreciated the placement and loading of landmarks ($S(++) = 3$; $S(+) = 2$). Moreover, the possibility to annotate the landmarks was emphasized of being helpful for the collaboration with other experts ($S(++) = 3$; $S(+) = 2$). One participant wished to have a temporal summary image of all placed landmarks.

Conclusion. All experts stated that they were able to use our tool without major problems and that they would definitely employ it for simultaneous evaluation of morphological and hemodynamic aneurysm parameters. After a short explanation of the exploration and navigation

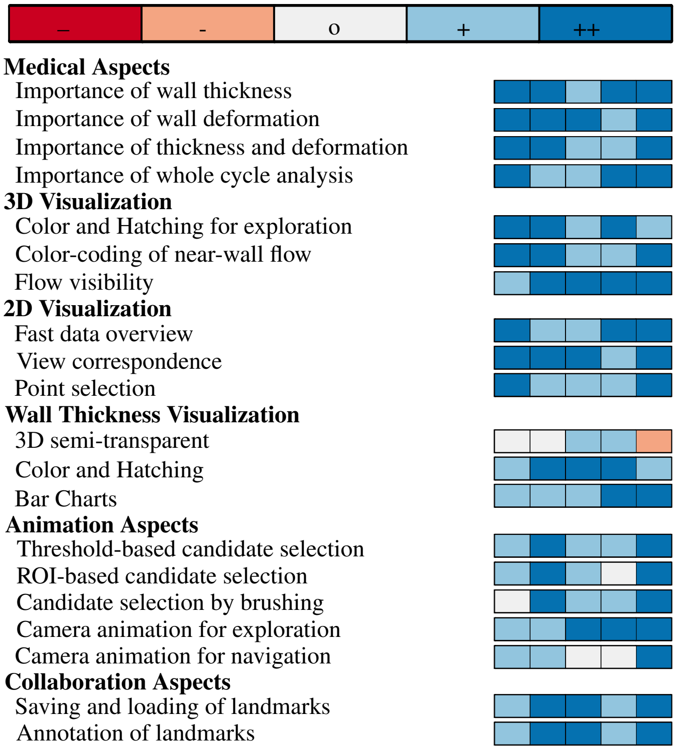

Fig. 8. The results of the evaluation with color-encoded Likert scores. Each box represents the answer of one subject: the two left-most boxes depict the physicians, the middle two boxes show the CFD experts, and the right-most box represents the medical visualization expert.

features, the participants were able to find suspicious regions on the surface. During evaluation, two main visualization techniques were described in depth: the 2.5D and 3D depiction that will be further discussed in the following. Next, minor improvements and suggestions are listed. Finally, we provide a short discussion for another application area to demonstrate the applicability of our method.

8 Discussion

We choose a 2D mapping of the 3D aneurysm surface to provide an occlusion-free overview depiction of the data. We restricted the mapping to the aneurysm and neglected outgoing vessels, since the experts are focused on the aneurysm. Therefore, we needed a parametrization of the mapping that preserves the round shape of the aneurysm. For this, the selected algorithm was suitable. However, there are distortions of the 2D flattening according to the parametrization, which is angle-preserving but not area-preserving. During the evaluation, we advised the experts of possible distortions. Due to the color-coding of the ostium in both views and the fact, that the 2D map serves as an overview depiction, the experts did not perceive possible distortions as cumbersome to get a first impression of the data. Similarly, the 3D bar chart should provide an overview depiction of a third scalar field. To handle possible occlusions by the bar chart, the user can optionally turn it off to see just the 2D map or rotate the 2.5D view. Alternative depictions such as two juxtaposed 2D maps would not lead to occlusions, but then the user would have to mentally combine three views, which is probably quite challenging. Another possibility would be the direct visualization of a third parameter in the 2D map using another color scale or iso-heightlines, but the visual perception of three parameters in one depiction is also very difficult.

Similar to the current exploration process, we provide a 3D depiction of the aneurysm surface, because the experts are familiar with such visualizations. For displaying two parameters simultaneously, experts prefer color-coding and cross hatching over 2D color maps, as discussed by Preim and Both [33].

Improvements. The experts wished to have more interaction in the 3D view. An interactive path line seeding, e.g., at morphologically conspicuous surface regions, would improve the analysis of near-wall flow patterns. Moreover, if the user selects a point on the vessel surface, the current active parameter values should additionally be listed. For the 3D bar charts, a quantification of their height using, for example, labels when the mouse hovers a bar would facilitate the exploration of the presented scalar field.

Domain Applications. Besides the rupture risk and treatment assessment, there are other possible application scenarios of our framework. Thus, our tool may also be helpful to explore the predicted blood flow after different treatment options, such as coiling and stenting. Another important application field is research and education of patients and students. Moreover, CFD and FSI play an essential role also in other vascular structures, such as the aorta, to better understand cardiovascular diseases. A common disease of the aorta is an abdominal aortic aneurysm. The amount of vessel wall deformation is even larger there and the solution presented here would probably be useful in these applications as well.

9 Conclusion and Future Work

We presented a framework for the analysis and exploration of cerebral aneurysms to improve the rupture risk evaluation. By providing a linked 2.5D and 3D aneurysm depiction, a simultaneous analysis of the aneurysm morphology such as wall thickness and deformation, hemodynamic and internal blood flow becomes possible for the first time. The combination of a 2D and 3D aneurysm visualization provides on the one hand a fast overview about the complex data and on the other hand a detailed exploration and assessment of rupture-prone parameters. The usage of modern visualization methods such as image-based hatching and automatic camera animations enable the detection of suspicious surface regions without a time-consuming manual search. All these methods put together, we present essential morphological and hemodynamic elements for the aneurysm rupture risk assessment in an integrated visualization. Thanks to our GPU implementation we achieve real-time rendering speeds even on mid-class computers. To evaluate our framework, we conducted a qualitative expert evaluation. This evaluation indicates that our overall approach is valid and applicable in medical research and other domains.

Although we evaluated our tool with positive feedback, some issues still need to be improved. First, the depiction of the tension inside the vessel should be improved to enable a more detailed exploration of the simulation results. At the moment, the stress tensor is reduced to a scalar field. However, a visualization would be important that depicts if the maximum tension occurs on the inner or outer wall. Furthermore, a depiction of the whole tensor using tensor glyphs would also be a helpful extension. Moreover, we should compare other mapping strategies that better preserve the aneurysm shape including adjacent vessels. This would be important for the analysis of different stent configurations and their influence on the blood flow in adjacent vessels. Finally, we would like to improve the FSI simulation by integrating real measured wall thickness values, which are expected soon.

Acknowledgments

This work was partially funded by the BMBF (STIMULATE:13GW0095A). The authors like to thank Uta Preim and Philipp Berg for the fruitful discussions on these and related topics.

References

[1] A. Baer, R. Gasteiger, D. Cunningham, and B. Preim. Perceptual Evaluation of Ghosted View Techniques for the Exploration of Vascular Structures and Embedded Flow. *Comput Graph Forum*, 30(3):811–20, 2011.

[2] Y. Bazilevs, M.-C. Hsu, Y. Zhang, W. Wang, X. Liang, T. Kvamsdal, R. Brekken, and J. G. Isaksen. A Fully-Coupled Fluid-Structure Interaction Simulation of Cerebral Aneurysms. *Comput Mech*, 46(1):3–16, 2010.

[3] P. Berg, C. Roloff, O. Beuing, S. Voss, and et al. The Computational Fluid Dynamics Rupture Challenge 2013–Phase II: Variability of Hemo-

dynamic Simulations in Two Intracranial Aneurysms. *J Biomech Eng*, 137(12):121008, 2015.

[4] R. Blankena, R. Kleinloog, B. Verweij, P. van Ooij, B. Ten Haken, Luijten, and et al. Thinner Regions of Intracranial Aneurysm Wall Correlate with Regions of Higher Wall Shear Stress: A 7T MRI Study. *Am J Neuroradiol*, 2016.

[5] S. Born, M. Pfeifle, M. Markl, M. Gutberlet, and G. Scheuermann. Visual Analysis of Cardiac 4D MRI Blood Flow Using Line Predicates. *IEEE Trans Vis Comput Graph*, 19:900–12, 2013.

[6] J. R. Cebral, F. Mut, J. Weir, and C. M. Putman. Association of hemodynamic characteristics and cerebral aneurysm rupture. *Am J Neuroradiol*, 32(2):264–70, 2011.

[7] J. R. Cebral, M. Vazquez, D. M. Sforza, G. Houzeaux, and et al. Analysis of Hemodynamics and Wall Mechanics at Sites of Cerebral Aneurysm Rupture. *J Neurointerv Surg*, 7(7):530–36, 2015.

[8] V. Costalat, M. Sanchez, D. Ambard, L. Thines, and et al. Biomechanical Wall Properties of Human Intracranial Aneurysms Resected Following Surgical Clipping. *J Biomech*, 44(15):2685–91, 2011.

[9] K. Crane, C. Weischedel, and M. Wardetzky. Geodesics in Heat: A New Approach to Computing Distance Based on Heat Flow. *ACM Trans Graph*, 32, 2013.

[10] S. M. Drucker. *Intelligent Camera Control for Graphical Environments*. PhD thesis, Massachusetts Institute of Technology, 1994.

[11] M. H. Everts, H. Bekker, J. B. T. M. Roerdink, and T. Isenberg. Illustrative Line Styles for Flow Visualization. In *Pac Graph SP*, 2011.

[12] R. Gasteiger, D. J. Lehmann, R. van Pelt, G. Janiga, O. Beuing, A. Vilanova, H. Theisel, and B. Preim. Automatic Detection and Visualization of Qualitative Hemodynamic Characteristics in Cerebral Aneurysms. *IEEE Trans Vis Comput Graph*, 18(12)(12):2178–87, 2012.

[13] R. Gasteiger, M. Neugebauer, O. Beuing, and B. Preim. The FLOWLENS: A Focus-and-Context Visualization Approach for Exploration of Blood Flow in Cerebral Aneurysms. *IEEE Trans Vis Comput Graph*, 17(12):2183–92, 2011.

[14] S. Glaßer, K. Lawonn, T. Hoffmann, M. Skalej, and B. Preim. Combined Visualization of Wall Thickness and Wall Shear Stress for the Evaluation of Aneurysms. *IEEE Trans Vis Comput Graph*, pages 2506–15, 2014.

[15] L. Goubergrits, J. Schaller, U. Kertzscher, N. van den Bruck, K. Poethkow, C. Petz, H. C. Hege, and A. Spuler. Statistical Wall Shear Stress Maps of Ruptured and Unruptured Middle Cerebral Artery Aneurysms. *J R Soc Interface*, 9(69):677–88, 2012.

[16] P. Hastreiter, B. Rezk-Salama, Ch.and Tomandl, K. E. W. Eberhardt, and T. Ertl. *Medical Image Computing and Computer-Assisted Interventation*, chapter Fast analysis of intracranical aneurysms based on interactive direct volume rendering and CTA, pages 660–69. 1998.

[17] M. Hayakawa, S. Maeda, A. Sadato, T. Tanaka, and et al. Detection of Pulsation in Ruptured and Unruptured Cerebral Aneurysms by Electrocardiographically Gated 3-Dimensional Computed Tomographic Angiography with a 320-row Area Detector Computed Tomography and Evaluation of its Clinical Usefulness. *J Neurosurg*, 69(4):843–851, 2011.

[18] G. Janiga, P. Berg, S. Sugiyama, K. Kono, and D. A. Steinman. The Computational Fluid Dynamics Rupture Challenge 2013—Phase I: prediction of rupture status in intracranial aneurysms. *Am J Neuroradiol*, 36(3):530–536, 2015.

[19] B. Köhler, R. Gasteiger, U. Preim, H. Theisel, M. Gutberlet, and B. Preim. Semi-automatic Vortex Extraction in 4D PC-MRI Cardiac Blood Flow Data using Line Predicates. *IEEE Trans Vis Comput Graph*, 19(12):2773–82, 2013.

[20] R. Lall, C. Eddleman, B. Bendok, and H. Batjer. Unruptured Intracranial Aneurysms and the Assessment of Rupture Risk based on Anatomical and Morphological Factors: Sifting through the Sands of Data. *Neurosurg Focus*, 26(5):E2, 2009.

[21] K. Lawonn, R. Gasteiger, and B. Preim. Adaptive Surface Visualization of Vessels with Animated Blood Flow. *Comput Graph Forum*, 33(8):16–27, 2014.

[22] K. Lawonn, S. Glaßer, A. Vilanova, B. Preim, and T. Isenberg. Occlusion-free Blood Flow Animation with Wall Thickness Visualization. *IEEE Trans Vis Comput Graph*, 22(1)(1):728–37, 2015.

[23] B. Lévy, S. Petitjean, N. Ray, and J. Maillot. Least squares conformal maps for automatic texture atlas generation. *ACM Trans Graph*, 21(3):362–71, July 2002.

[24] J. Ma, J. W. Walker, C. Wang, S. A. Kuhl, and C. Shene. Flowtour: An automatic guide for exploring internal flow features. In *IEEE PacificVis*, pages 25–32, 2014.

[25] O. Mattausch, T. Theußl, H. Hauser, and E. Gröller. Strategies for Interactive Exploration of 3D Flow Using Evenly-spaced Illuminated Streamlines. In *Proc. of SCCG*, pages 213–22, 2003.

[26] H. Meng, V. M. Tutino, J. Xiang, and A. Siddiqui. High wss or low wss? complex interactions of hemodynamics with intracranial aneurysm initiation, growth, and rupture: Toward a unifying hypothesis. *Am J Neuroradiol*, 35:1254–62, 2013.

[27] T. Mönch, M. Neugebauer, and B. Preim. Optimization of Vascular Surface Models for Computational Fluid Dynamics and Rapid Prototyping. In *International Workshop on Digital Engineering*, pages 16–23, 2011.

[28] K. Mühler, M. Neugebauer, C. Tietjen, and B. Preim. Viewpoint Selection for Intervention Planning. In *IEEE/Eurographics Symposium on Visualization*, pages 267–74, 2007.

[29] M. Neugebauer, R. Gasteiger, O. Beuing, V. Diehl, M. Skalej, and B. Preim. Map Displays for the Analysis of Scalar Data on Cerebral Aneurysm Surfaces. In *Comput Graph Forum*, volume 28 (3), pages 895–902, 2009.

[30] M. Neugebauer, K. Lawonn, O. Beuing, P. Berg, G. Janiga, and B. Preim. AmniVis - A System for Qualitative Exploration of Near-Wall Hemodynamics in Cerebral Aneurysms. *Comput Graph Forum*, 32(3):251–60, 2013.

[31] S. Oeltze, D. J. Lehmann, A. Kuhn, G. Janiga, H. Theisel, and B. Preim. Blood Flow Clustering and Applications in Virtual Stenting of Intracranial Aneurysms. *IEEE Trans Vis Comput Graph*, 20(5):686–701, 2014.

[32] E. Oubel, M. De Craene, C. M. Putman, J. R. Cebral, and A. F. Frangi. Analysis of intracranial aneurysm wall motion and its effects on hemodynamic patterns. In *Proc. of SPIE*, volume 6511, pages 65112A–65112A–8, 2007.

[33] B. Preim and C. Botha. *Visual Computing for Medicine*. Morgan Kaufmann, 2 edition, 2013.

[34] S. Rusinkiewicz. Estimating Curvatures and Their Derivatives on Triangle Meshes. In *3DPVT*, pages 486–93, 2004.

[35] T. Salzbrunn and G. Scheuermann. Streamline Predicates. *IEEE Trans Vis Comput Graph*, 12(6):1601–12, 2006.

[36] M. Sanchez, D. Ambard, V. Costalat, S. Mendez, F. Jourdan, and F. Nicoud. Biomechanical assessment of the individual risk of rupture of cerebral aneurysms: A proof of concept. *Ann Biomed Eng*, 41(1):28–40, 2013.

[37] M. Sanchez, O. Ecker, D. Ambard, F. Jourdan, and et al. Intracranial aneurysmal pulsatility as a new individual criterion for rupture risk evaluation: Biomechanical and numeric approach. *Am J Neuroradiol*, 35(9):1765–71, 2014.

[38] J. Schöberl. An Advancing Front 2D/3D- Mesh Generator Based On Abstract Rules. *Comput Vis Sci*, 1:41–52, 1997.

[39] J. Tao, X. Huang, F. Qiu, C. Wang, J. Jiang, C.-K. Shene, Y. Zhao, and D. Yu. VesselMap: A web interface to explore multivariate vascular data. *Computers & Graphics*, 2016.

[40] B. Tomandl, P. Hastreiter, S. Iserhardt-Bauer, N. C. Köstner, and et al. Standardized evaluation of CT angiography with remote generation of 3D video sequences for the detection of intracranial aneurysms. *Radiographics*, 23(2):e12, 2003.

[41] A. Valencia, D. Ledermann, R. Rivera, E. Bravo, and et al. Blood flow dynamics and fluid-structure interaction in patient-specific bifurcating cerebral aneurysms. *INT J NUMER METH FL*, 58(10):1081–1100, 2008.

[42] R. van Pelt, J. O. Bescós, M. Breeuwer, R. E. Clough, M. E. Gröller, B. ter Haar Romeny, and A. Vilanova. Exploration of 4D MRI Blood Flow using Stylistic Visualization. *IEEE Trans Vis Comput Graph*, 10(6):1339–47, 2010.

[43] R. van Pelt, J. O. Bescós, M. Breeuwer, R. E. Clough, M. E. Gröller, B. ter Haar Romeny, and A. Vilanova. Interactive Virtual Probing of 4D MRI Blood-Flow. *IEEE Trans Vis Comput Graph*, 17(12):2153–62, 2011.

[44] R. van Pelt, R. Gasteiger, K. Lawonn, M. Meuschke, and B. Preim. Comparative Blood Flow Visualization for Cerebral Aneurysm Treatment Assessment. *Comput Graph Forum*, 33(3)(3):131–40, 2014.

[45] R. van Pelt, S. Jacobs, B. ter Haar Romeny, and A. Vilanova. Visualization of 4D Blood-Flow Fields by Spatiotemporal Hierarchical Clustering. *Comput Graph Forum*, 31(3pt2):1065–74, 2012.

[46] P. P. Vázquez, M. Feixas, M. Sbert, and W. Heidrich. Viewpoint selection using Viewpoint Entropy. In *Proc. of VMV*, pages 273–80, 2001.

[47] P. P. Vázquez, M. Feixas, M. Sbert, and W. Heidrich. Automatic View Selection Using Viewpoint Entropy and its Application to Image-Based Modeling. *Comput Graph Forum*, 22(4):689–700, 2003.